JOURNAL OF NANO- AND ELECTRONIC PHYSICS
Vol. 17 No 3, 03035(7pp) (2025)

ЖУРНАЛ НАНО- ТА ЕЛЕКТРОННОЇ ФІЗИКИ
Том 17 № 3, 03035(7cc) (2025)

OPEN ACCESS

REGULAR ARTICLE

First-Principles Calculation Investigations of Bandgap Bowing Parameters, Electronic and Optical Properties of $Cd_{1-x}Zn_xTe$, $Cd_{1-x}Zn_xSe$ and $Cd_{1-x}Zn_xS$ Semiconductors Alloys

K. Mimouni[1], K. Beladjal[1], Slimane Latreche[2], Charef Azzeddine[1,3,*] ✉, A. Benzetta[4], M. Abderrezek[5], N. Mokdad[1], Benramache Said[3]

[1] *Laboratoire d'Étude des Matériaux Optoélectronique & Polymères, Physics Department, University Oran1, Ahmed Ben Bella, BP1524 El M'naour, Oran, Algeria*
[2] *Technical Platform for Physico-Chemical Analysis (PTAPC), Microstructural and Microanalysis Division, University of Science and Technology (USTHB), BP 32 El-Alia, Bab-Ezzouar, Algiers 16111, Algeria*
[3] *Laboratoire de Physique Photonique et Nanomatériaux Multifonctionnels, LPPNM, Biskra University, Biskra 07000 Algeria*
[4] *Higher School of Signals (HSS), Po Box 11, Kolea, 42070, Tipaza, Algeria*
[5] *Unité de Développement des Equipements Solaires, UDES / Centre de Développement des Energies Renouvelables, CDER, 42415Tipaza, Algérie*

(Received 18 March 2025; revised manuscript received 20 June 2025; published online 27 June 2025)

In this study, we conducted a detailed examination of the energy band gaps in semiconductor alloys, specifically $Cd_{1-x}Zn_xTe$, $Cd_{1-x}Zn_xSe$, and $Cd_{1-x}Zn_xS$, all of which adopt the zinc-blende crystal structure. To carry out our analysis, we used the full-potential linearized augmented plane wave (FP-LAPW) method, applying both the generalized gradient approximation (GGA) and local density approximation (LDA) to achieve accurate results. For precise determination of band gaps and the bowing parameters, we relied on the Tran-Blaha modified Becke-Johnson (TB-mBJ) exchange potential, known for its effectiveness in band structure calculations. Our results showed a moderately nonlinear dependence of band gap values on composition, with bowing parameters estimated at approximately $b \approx 0.49$ eV for $Cd_{1-x}Zn_xTe$, $b \approx 0.68$ eV for $Cd_{1-x}Zn_xS$, and $b \approx 0.63$ eV for $Cd_{1-x}Zn_xSe$. This observed nonlinearity was mainly attributed to volume deformation effects, following the Zunger approach, which explains how structural distortions can impact electronic properties. Beyond band gap analysis, we examined key optical properties, including the absorption coefficient, refractive index, reflectivity, energy loss function, and oscillator strength. These optical characteristics offer deeper insights into the materials' electronic structures and response to light. Interestingly, we observed an increase in the effective electron numbers during photoexcitation as the Zn concentration rose, indicating enhanced optical activity in these alloys. This study sheds light on both electronic and optical properties, making these $Cd_{1-x}Zn_xTe$, $Cd_{1-x}Zn_xSe$, and $Cd_{1-x}Zn_xS$ alloys promising candidates for optoelectronic applications where fine-tuning of band gaps and optical responses is essential for optimal device performance.

Keywords: Energy gap, Bowing parameters, Optical properties, II-VI semiconductors, Tran-Blaha modified Becke-Johnson exchange potential.

DOI: 10.21272/jnep.17(3).03035 PACS number: 71.20.Nr

1. INTRODUCTION

The Recently, there has been growing interest in II-VI Cadmium-containing alloys for their potential applications in electronics and optoelectronics devices like LEDs, lasers, optical fibers, and photovoltaics [1]. These materials offer several advantages over traditional semiconductors like silicon and germanium, which have fixed and indirect band gaps. The bandgap of MX compounds (M = Zn, Cd and X = S, Se, Te) can be adjusted from 1.5 eV in CdTe, 1.80 eV in CdSe, 2.5 eV in CdS, 2.39 eV in ZnTe, 2.7 eV in ZnSe and 3.7 eV in ZnS by varying the alloy composition [2].

Binary CdTe, ZnTe, and their ternary alloys have been extensively studied and utilized in various applications such as nuclear medicine, solar cells, medical imaging, environmental monitoring, X-ray, and gamma-ray detectors. Various techniques including epitaxy [3], liquid phase epitaxy, electrode position, close space vapors transport, laser ablation [6], thermal vapor evaporation, sputtering, Bridgman method, and metal–organic chemical vapor deposition (MOCVD), have been employed for the successful growth of CdZnTe films [2].

Cadmium Sulfide (CdS) is a direct band gap semiconductor with a band gap energy of 2.42 eV, making it ideal for manufacturing CdTe and CuInSe solar cell thin films. CdZnS ternary alloy, formed by replacing Zn ions with Cd ions in the CdS lattice, enhances photocurrent, reduces absorption loss of the window layer, and increases spectral response. Various methods such as vacuum evaporation, radio frequency (RF) magnetron sputtering, RF co-sputtering using different RF-power ratios of CdS and ZnS, Chemical bath deposition (CBD) have

---

[*] Correspondence e-mail: azzoucharef3@gmail.com

© 2025 The Author(s). Journal of Nano- and Electronic Physics published by Sumy State University. This article is distributed under the terms and conditions of the Creative Commons Attribution (CC BY) license.

Cite this article as: K. Mimouni, et al., *J. Nano- Electron. Phys.* 17 No 3, 03035 (2025) https://doi.org/10.21272/jnep.17(3).03035

been used for synthesizing CdZnS films [3].

However, CdSe is prone to photo-corrosion in photoelectrochemical cells, while ZnSe is more stable due to its wide band gap and low light activity To address this issue, CdSe and ZnSe can be combined to form a $Cd_{1-x}Zn_xSe$ ternary alloy. These materials allow customization of energy band gap and lattice parameters independently, enabling the production of new semiconductor materials suitable for increasing solar spectrum absorption and enhancing light corrosion resistance.

Comparative analysis shows that ab-initio calculations using Tran Blaha modified Beck-Johnson exchange potential yield superior results compared to other theoretical techniques and closely match experimental measurements. This method is promising for band gap engineering in II-VI semiconductors, providing accurate band structure results and orbital states location. The effectiveness of this approach is attributed to proper treatment of d orbitals in highly correlated electron systems. The origin of bowing parameters is briefly discussed in terms of volume deformation between parent links

2. CALCULATION METHOD

Calculations rely on solving the Kohn-Sham equations self-consistently within the framework of density functional theory (DFT), employing the full potential linearized augmented plane wave method as implemented in the Wien2k code. Both local density and generalized gradient approximations were used to account for the exchange and correlation contributions [30]. Additionally, we utilized a semi-local Tran Blaha modified Becke-Johnson exchange potential, TB-mBJ, to provide an accurate description of the electronic properties. This potential, as described in reference [29], was incorporated into our calculations:

$$v^{mBJ}_{x,\sigma}(r) = c\,v^{BR}_{x,\sigma}(r) + (3c-2)\frac{1}{\pi}\sqrt{\frac{5}{12}}\sqrt{\frac{2t_\sigma(r)}{\rho_\sigma(r)}} \qquad (1)$$

The first term $v^{BR}_{x,\sigma}(r)$ is Becke-Roussel potential [29], $t_\sigma(r)$ is the kinetic energy, $\rho_\sigma(r)$is the electron density and the parameter c are defined by the following equation:

$$c = \alpha + \beta\left(\frac{1}{V_{cell}}\int\frac{|\nabla\rho(r')|}{\rho(r')}d^3r'\right)^{1/2} \qquad (2)$$

Where α, β are empirical parameters and V_{cell} is the crystal unit cell volume.

The advantage of this method is that it does not require any special computational effort and is even slightly more complex than traditional GGA and LDA methods. Furthermore, the implementation accuracy of various DFT-based methods is comparable to that of advanced methods. To simulate ternary alloys, we used a 16-atom $1 \times 1 \times 1$ supercell that doubled the size of the original unit cell in the basal plane. The cutoff parameter for the linearized extended plane wave basis is KMAX = 8/RMT, while the energy separation between valence and nuclear states is – 6 Ry. For irreducible Brillouin zone sampling, we use 1500 k points for binary alloys and 100 k points for ternary alloys. The charge density is then extended by Fourier transform to Gmax = 12 Ry for LDA and Gmax = 14 Ry for GGA.

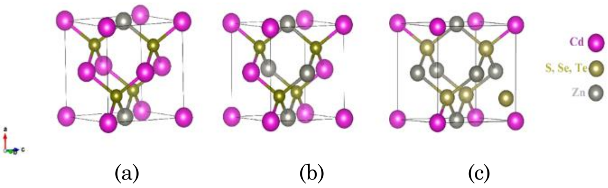

Fig. 1 – The ternary compounds $Cd_{1-x}Zn_xY$ (S, Se and Te) crystal structure of the form Zinc blende (a) $x = 0.25$; (b) $x = 0.5$ and (c) $x = 0.75$

In the zinc blende crystal structure, also known as the ZB structure, atoms are arranged in a tetrahedral pattern where each atom is surrounded by four nearest neighbors. The tetrahedrons are stacked on top of each other in a repeating pattern to form the crystal structure.

In ternary compounds, there are three types of atoms present in the crystal structure. In the zinc blende structure, these atoms will be arranged in a regular pattern, with one type of atom occupying the tetrahedral sites and the other two types of atoms occupying the octahedral sites[2]. The exact arrangement of atoms in a ternary compound will depend on the specific chemical composition and the relative sizes of the atoms.

3. RESULTS AND DISCUSSION

With the aim of providing basic knowledge of the concept and application of future energy gap devices based on zinc and Cadmium compound II-VI semiconductors. The electronic band structure of these compounds was estimated. Consequently, Table 1 lists the energy gap, at Γ point, calculated the two approximations of GGA and LDA with modified Becke and Johnson (mBJ). This table and Figures 2 and 3 outline the band structure of Zinc Blend of binary MX (M = Zn, Cd and X = S, Se, Te) assessed with both GGA and GGA- TB-mBJ. Predictably, these materials represent the direct band gap at the center of the Brillouin zone.

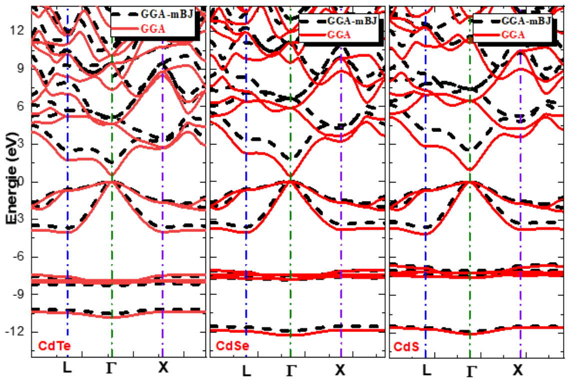

Fig. 2 – Electronic bands structures of binary Cadmium's semiconductors CdTe, CdSe and CdS calculated by within GGA (solid line) and GGA-mBJ (dash line)

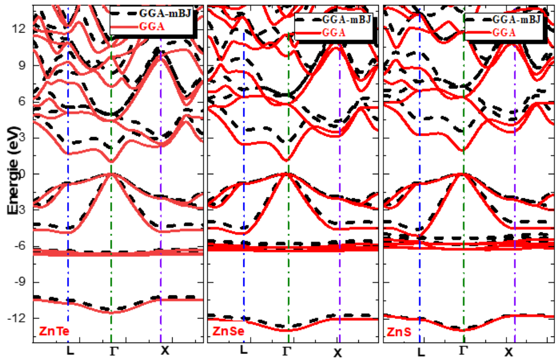

Fig. 3 – Electronic bands structures of binary Zincs semiconductors ZnTe, ZnSe and ZnS calculated within GGA (solid line) and GGA-mBJ (dash line)

Table 1 – Energy band gap of MX (M = Zn, Cd and X = S, Se, Te) together with theoretical and experimental results[1, 4, 5, 8, 9]

	Present	Experimental	mBJ	Theory	GW
CdTe	0.541[a], 0.56857[b] 1.5584[c], 1.80938[d]	1.43[e],1.92[f],1.5[g],1.60[i],1.43[k] 1.50[l],1.43[m],1.60[o],1.61[p]	1.56[q] 1.68[r]	0.80[i],0.58[t],0.74[s] 0.49[u], 1.75[u],1.33[v]	1.76[i],1.22[s] 1.47[s]
CdSe	0.48015[a], 0.37292[b] 1.79597[c],1.97914[d]	1.90[f], 1.8[h], 1.90[i],1.75[k] 1.70[l],1.74[m],1.82[o],1.70[p]	1.89[q] 1.84[r]	0.76[i],0.48[t],0.88[s] 0.32[u],1.89[u],1.35[v]	2.01[i],1.25[s] 1.56[s]
CdS	0.96264[a], 0.92275[b] 2.52061[c], 2.67944[d]	2.49[e], 2.59[f], 2.55[i], 2.5[j] 2.485[k], 2.40[l], 2.49[m], 2.58[o] 2.48[p]	2.66[q] 2.56[r]	1.37[i],1.00[t],1.82[s] 0.85[u],2.60[u],1.92[v]	2.83[i], 2.11[s] 2.47[s]
ZnTe	1.01317[a], 1.20071[b] 2.16955[c], 2.55851[d]	2.39[e], 2.39[i], 2.26[k], 2.10[l] 2.39[m], 2.39[o], 2.39[p]	2.22[q] 2.4[r, f]	1.33[i],1.07[t], 0.21[s] 1.16[u], 1.41[u],1.78[v]	2.57[i],1.98[s] 2.26[s]
ZnSe	1.10705[a], 1.20279[b] 2.58438[c], 2.8913[d]	2.69[e], 2.82[i], 2.7[k], 2.58[l] 2.69[m], 2.87[o], 2.82[p]	2.67[q] 2.7[r]	1.45[i],1.14[t], 0.17[t] 1.26[u], 2.82[u], 2.2[v]	2.84[i], 2.24[s] 2.58[s]
ZnS	1.96147[a], 2.07981[b] 3.54677[c], 3.8484[d]	3.1[e],3.78[i], 3.68[k], 3.70[l] 3.61[m], 3.82[o], 3.84[p]	3.66[q] 3.6[r]	2.37[i], 2.00[t],0.80[s] 2.07[u], 3.82[u],3.27[v]	3.98[i], 3.38[s] 3.80[s]

[a, b] GGA/LDA results, [c, d] GGA-mBJ/LDA-mBJ results.

The previous table proves that the TB-mBJ result is close to experimental results. Moreover, the result obtained for CdX (S, Se and Te) by mBJ aligned with the experimental values, compared to the recent reported mBJ. The experimental band gap of ZnSe in the zinc Blende phase is 2.58 eV, while in the GGA-mBJ calculation it equals 2.5844 eV. Indeed, ZnS demonstrates excellent results obtained by the LDA mBJ, which equals 3.8484 eV compared with the experimental 3.84 eV. The gap between binary Cd and Zn is greatly underestimated in conventional GGA and LDA calculations.

The energy gap of the $Cd_{1-x}Zn_xTe$ increases with the Zn molar fraction due to the smaller gap of Zn atoms compared to Cd atoms, enhancing the cations-anions electronegativity. Table 1 provides a comparison between the calculated band gap energy, the experimental and theoretical report data. It is evident that the study's results using the GGA-mBJ of binary compounds CdTe and ZnTe, are consistent with the experimental measurements . It is also obvious from table1 that the binary compound results are consistent with the theoretical results calculated using mBJ.

The alloy band gap values of $Cd_{1-x}Zn_xTe$ reported results in Figure 4 are comparable with the experimentally measured Ammar, Franc, Poon, and in good correlation with other theoretical calculations B.B. Dumre and others.

The energy gap variations deviate slightly from linear dependence, displaying a downward bowing $b = 0.46$ eV calculated with GGA-mBJ. Furthermore, the degree of deflection indicates the degree to which the crystal field fluctuates or the degree to which nonlinear effects occur due to the anisotropic nature of the bond, the bowing parameter of $b = 0.46$ eV for the $Cd_{1-x}Zn_xTe$ alloys in the present work correlates with other experimental and theoretical calculations. The bowing parameter of $b = 0.46$ eV is calculated using the quadratic fit equation, quantifying the deviation from the Vegard law is described by the flowing equation [7]:

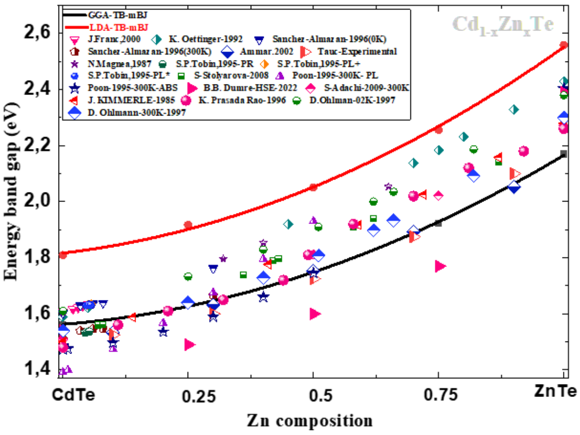

Fig. 4 – Energy band gaps of $Cd_{1-x}Zn_xTe$ alloy as a function of Zinc content together with experimental results

$$Eg_{ABC} = Eg_{AB}\,x + Eg_{BC}(1-x) - b\,x(1-x). \qquad (3)$$

Where, $Eg_{ABC}, Eg_{AB}, Eg_{BC}$ are the energy band gaps of the CdX and ZnX (X = S, Se, Te) alloys, and b is the bowing parameter describing the deviation from the Vegard law.

$$Cd_{1-x}Zn_x\mathrm{Te} = \begin{cases} E_g^{GGA-mBJ} = 1{,}56254 + (0{,}14143)\mathrm{x} + (0{,}46187)\mathrm{x}^2 \\ E_g^{LDA-mBJ} = 1.81676\ + (0.20809)\mathrm{x} + (0.52689\,)\mathrm{x}^2 \end{cases} \qquad (4)$$

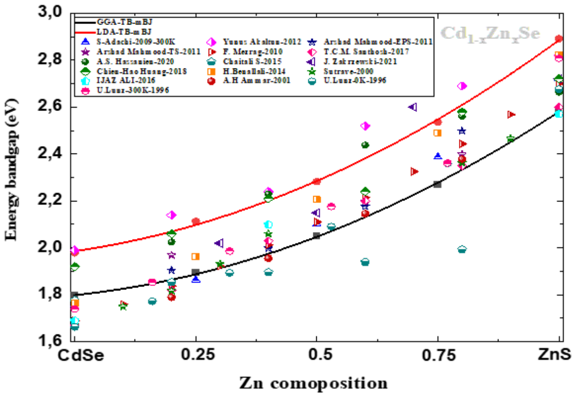

Fig. 5 – Energy band gap of $Cd_{1-x}Zn_xSe$ alloy as a function of Zinc content together with experimental results

It is depicted by Figure 5 that the energy band gap of $Cd_xZn_{1-x}Se$ alloy as a function of the molar fraction for both Zinc-Blende crystal types aligns with the experimentally measured by U. Lunz, Ammar, Sutrave, Chien-Hao Huang, Benallali, Ahmed Saeed Hassanien, Yunus Akaltun and J. Zakrzewski; are also shown in comparison. These results also correlate with other theoretical calculations [10].

It has been reported that ternary compound semiconductors such as CdZnSe band gap is closely related to individual band gaps of the component materials of ternary compound semiconductors. In the current situation, it depends on the band gaps of CdSe and ZnSe. Nevertheless, the band gap of the crystal Ternary joins deviates from linear and second order because of crystal periodicity discontinuities and lattice mismatch. The effect determines the band gap of the ternary compound. It is possible to assess the second-order effects, known as arc parameters, from the parabolic fit of the band gap with the x content in the ternary compound. As shown in Figure 4, the CdZnSe band gap varies with the zinc concentration (*x*). Additionally, the bowing parameter where *b* = 0.48 is calculated with GGA-mBJ, the band gap extent variation could be defined by introducing the energy band gap value to a quadratic equation as follow [11]:

$$Cd_{1-x}Zn_xSe = \begin{cases} E_g^{GGA-mBJ} = 1.81743 + (0.26566)\mathrm{x} + (0.48702)\mathrm{x}^2 \\ E_g^{LDA-mBJ} = 1.98619 + (0.2969)\mathrm{x} + (0.60201)\mathrm{x}^2 \end{cases} \tag{5}$$

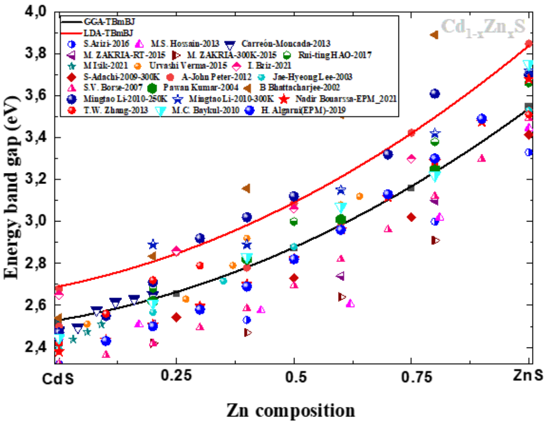

Fig. 6 – Energy band gap of Cd1 – *x*Zn*x*S alloy as a function of Zinc content together with experimental results

The previous Figure 6 presents the compositional dependence of Cd*x*Zn1 – *x*S energy band gap for both Zinc-Blende crystal-types. At both the extremes (CdS and ZnS) the study finding aligned with the experimentally measured previously presented by John Peter. V. Kumar, P. Kumar, Jae Hyeong-Lee, Mingtao Li and M.C. Baykul. Therefore, mBJ exchange potential has been proven to be effective in treating CZS band gaps and provides estimates that correlate with other theoretical calculations H. Algarni. The bowing parameter b is also calculated using the quadratic fit equation. The currently calculated b value is 0.69 eV calculated with LDA-mBJ, and 0.90 eV calculated with LDA, which is consistent with the experimentally measured value of 0.80 eV. These values confirm that the study results are far better than the other calculated results. That the reason for the reasonable band gap bending coefficient is the logical theoretical band gap of CZS.

$$Cd_{1-x}Zn_xS = \begin{cases} E_g^{GGA-mBJ} = 2.5299 + (0.37721)\mathrm{x} + (0.63114)\mathrm{x}^2 \\ E_g^{LDA-mBJ} = 2.69591 + (0.45196)\mathrm{x} + (0.69061)\mathrm{x}^2 \end{cases} \tag{6}$$

With the aim of understanding the physical origin of the bowing parameters inside A1 – *x*B*x*C, the study follows the Zunger et al., approach, and breaks up the total bowing parameter *b* into physically distinct contributions.

Table 2 – Decomposition of the bowing parameter into volume deformation (VD), charge exchange (CE) and structural relaxation (SR) contributions for the Cd1 – *x*Zn*x*Y (Y = Te, Se and S) ternary alloy (all values in eV) [12, 13].

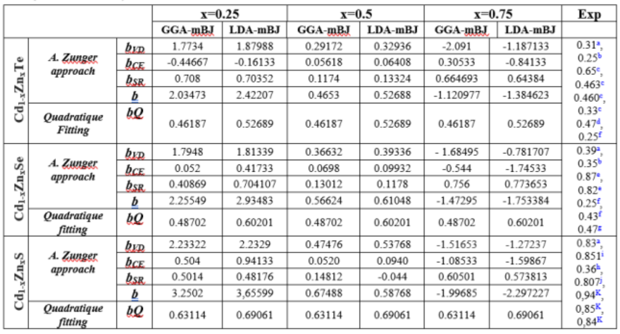

			x=0.25		x=0.5		x=0.75		Exp
			GGA-mBJ	LDA-mBJ	GGA-mBJ	LDA-mBJ	GGA-mBJ	LDA-mBJ	
$Cd_{1-x}Zn_xTe$	*A. Zunger approach*	b_{VD}	1.7734	1.87988	0.29172	0.32936	-2.091	-1.187133	0.31[a], 0.25[b] 0.65[c], 0.463[c] 0.460[c], 0.33[c] 0.47[d], 0.25[f]
		b_{CE}	-0.44667	-0.16133	0.05618	0.06408	0.30533	-0.84133	
		b_{SR}	0.708	0.70352	0.1174	0.13324	0.664693	0.64384	
		b	2.03473	2.42207	0.4653	0.52688	-1.120977	-1.384623	
	Quadratique Fitting	bQ	0.46187	0.52689	0.46187	0.52689	0.46187	0.52689	
$Cd_{1-x}Zn_xSe$	*A. Zunger approach*	b_{VD}	1.7948	1.81339	0.36632	0.39336	- 1.68495	-0.781707	0.39[a], 0.35[b] 0.87[e], 0.82[e] 0.25[f], 0.43[f] 0.47[g]
		b_{CE}	0.052	0.41733	0.0698	0.09932	-0.544	-1.74533	
		b_{SR}	0.40869	0.704107	0.13012	0.1178	0.756	0.773653	
		b	2.25549	2.93483	0.56624	0.61048	-1.47295	-1.753384	
	Quadratique fitting	bQ	0.48702	0.60201	0.48702	0.60201	0.48702	0.60201	
$Cd_{1-x}Zn_xS$	*A. Zunger approach*	b_{VD}	2.23322	2.2329	0.47476	0.53768	-1.51653	-1.27237	0.83[a], 0.851[i] 0.36[h], 0.807[j], 0,94[K], 0,85[K], 0,84[K]
		b_{CE}	0.504	0.94133	0.0520	0.0940	-1.08533	-1.59867	
		b_{SR}	0.5014	0.48176	0.14812	-0.044	0.60501	0.573813	
		b	3.2502	3,65599	0.67488	0.58768	-1.99685	-2.297227	
	Quadratique fitting	bQ	0.63114	0.69061	0.63114	0.69061	0.63114	0.69061	

The first stage measures the volume deformation (VD) effect on bowing. The corresponding contribution b_{VD} with bowing parameter represents the relative response of the band structure of the binary compounds AC and BC to the hydrostatic pressure, which results here from the change of their various equilibrium lattice constants to the alloy value. The second contribution is the charge exchange (CE) contribution b_{CE} that reflects the effect of taxation required due to the behavior difference of the connection to the lattice constant *a*. The final stage, the "structural relaxation" (SR), measures the changes of the relaxed alloy b_{SR}. Consequently, the total bowing parameter is defined as

$$b = b_{VD} + b_{CE} + b_{SR} \tag{7}$$

This allows a division of all the bowing b into three contributions according to:

$$b_{VD} = \frac{\left(E_g(AC_{Cal}) - E_g(AC_{VCA})\right)}{1-x} + \frac{\left(E_g(BC_{Cal}) - E_g(BC_{VCA})\right)]}{x} \tag{8}$$

$$b_{CE} = \frac{E_g(AC_{VCA})}{1-x} + \frac{E_g(BC_{VCA})}{x} - \frac{E_g(ABC_{VCA})}{x*(1-x)} \tag{9}$$

$$b_{SR} = \frac{[E_g(ABC_{VCA}) - E_g(ABC_{Cal})]}{x*(1-x)} \tag{10}$$

Table 2, provides a summary of each contribution calculation at the middle range. This table also demonstrate that the bowing effect was arising mainly from the volume deformation due the strong lattice mismatch between binary parent compounds. This mismatch lead also to significant structural relaxations while, the charge transfer effect was neglected. The bowing parameters are listed in Table 2 in comparison with experiments. It is interesting to note that the main experimental results are in fall between our GGA/LDA-TB-mBJ calculations. To the same weight for all ternary sulfide alloys, the volume deformation was basically involved for the bowing effect while other contributions are relatively weak.

The energy gaps derived from Eqs. (7) to (10) were computed based on the specified atomic structures and lattice constants. Table 2 presents our findings for the bowing parameter, denoted as *b*, at *x* = 0.25, 0.5, and 0.75. Our calculations using GGA-mBJ reveal a composition-dependent behavior in the bowing parameter,

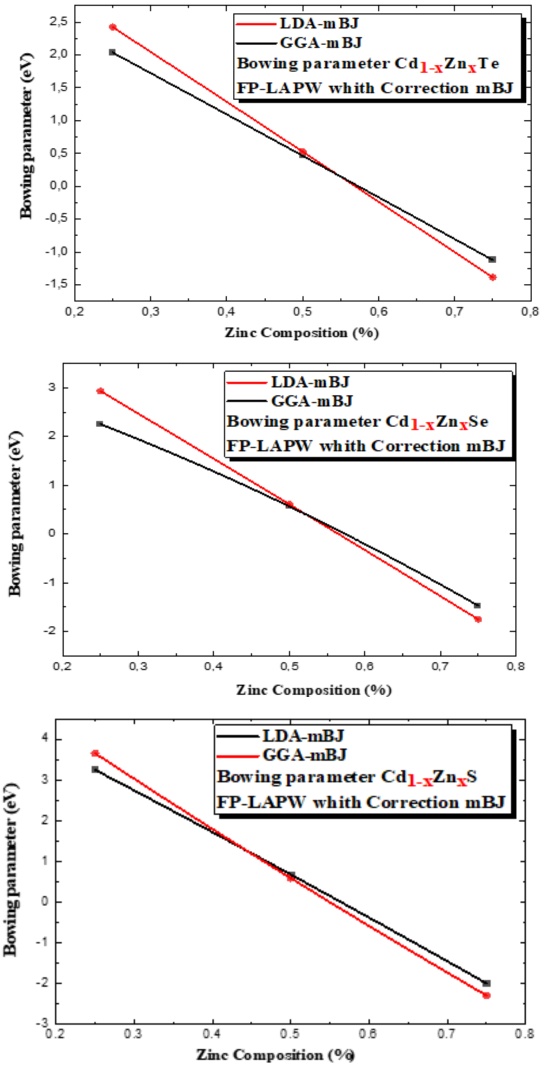

Fig. 7 – Calculated bowing parameter as a function of Zn composition using LDA-mBJ (solid squares) and GGA-mBJ (solid circles) of Cd$_{1-x}$Zn$_x$Y (Y = Te, Se and S) ternary alloys

which differs from the results obtained using LDA-mBJ calculations, where a weak composition dependence is observed. Figure 7 illustrates the variation of the bowing parameter with concentration. It demonstrates that the bowing remains linear. Specifically, for the Cd$_{1-x}$Zn$_x$Te alloy, the bowing parameter ranges from 2.42 eV (x = 0.25) to – 1.38 eV (x = 0.75). Similarly, for the Cd$_{1-x}$Zn$_x$Se alloy, it ranges from 2.93 eV (x = 0.25) to – 1.73 eV (x = 0.75), and for the Cd$_{1-x}$Zn$_x$S alloy, it extends from 3.65 eV (x = 0.25) to – 2.29 eV (x = 0.75). The significance of the bowing parameter b(VD) can be linked to the difference in lattice constants of the binary compounds. The primary contribution to the bowing parameter is attributed to the effect of volume deformation, except for x = 0.75, where the contribution of relaxation (b(SR)) was found to be larger than b(VD). This contribution stems from volume deformation and the electronegativity difference among the atoms in the Cd$_{1-x}$Zn$_x$Y (Y = Te, Se, and S) ternary alloys. The bowing parameter is a crucial consequence of the exchange of load between constituents.

In summary, our calculations indicate that volume deformation and electronegativity have a notable impact on the bowing parameter of the Cd$_{1-x}$Zn$_x$Y (Y = Te, Se, and S) ternary alloys [14].

4. OPTICAL PROPERTIES FOR CdZnX (S, Se AND Te)

In this section, the study considers the optical properties for CdZnX (S, Se and Te), by applying the FP-LAPW method, implemented in Wien2k code. The ability of a material to exhibit induced polarization or magnetization at selected wavelengths and its internal structure details could be provided by optical spectra. Moreover, several techniques such as Ellipsometry, reflection, absorption, cathodoluminescence, and photoluminescence are frequently used to characterize different materials. It is worthwhile to state that the wide range of band gaps (1.50 – 3.8) for CdZnX (S, Se and Te), comprised in the near-infrared and visible range, is more suitable for many technical applications than the fixed band gap of binary compounds. Therefore, the knowledge of the band gap engineering and optical properties of materials is of special importance in the design and analysis of materials [15]. Figure 8 demonstrates that the absorption coefficients α(x) of CdZnX (S, Se and Te) (0.25 ≤ x ≤ 0.75) are plotted against different incident photon energies. All the other optical constants, such as the refractive index $n(\omega)$, coefficient extinctions $k(\omega)$, reflectivity $R(\omega)$, electron energy-loss spectrum $L(\omega)$ and the dielectric function.

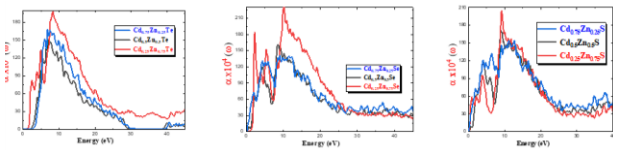

Fig. 8 – Frequency dependent absorption coefficient of CdZnX (S, Se and Te)

The calculated refractive indices and coefficient extinctions of CdZnX (S, Se and Te) for each composition x (0.25 ≤ x ≤ 0.75) are presented in Figure 8. It is well presented that the Zn concentration in CdX (S, Se and Te) induces the refractive index of the material at zero frequency to decrease. This figure also confirms the inverse relationship of this index with the band gap CdZnX (S, Se and Te) [16]. Moreover, it is obvious that the normal refractive index increases as the photon frequency increases from the zero-frequency limit. A peak point is reflecting an inter-band transition at Γ-Γ. While, a lower energy hump corresponds to the basic band gap. The dispersion curves of the refractive indices are described in Figure 9 for each composition x, and the refractive index n(0) for Cd$_{1-x}$Zn$_x$Te is found to be 2.4, 2.5 and 2.45. The Zn concentration x increases in CdTe increases; the value of the refractive index decreases in the range of 0-6 eV [17].

The dispersion curves $n(v)$ for Cd$_{1-x}$Zn$_x$Se of each composition x, and the values of refractive index n(0) equal 2.16, 2.55 and 2.62 respectively. Furthermore, as the Zn concentration x increases in CdSe, the value of the refractive index decreases in the range of 0-4.5 eV [18].

The dispersion curves ($n(v)$) for Cd$_{1-x}$Zn$_x$S are described in Figure 8 for each composition x, and the values of the refractive index $n(0)$ equal 3.26, 2.5 and 2.87 respectively. Similarly, as the Zn concentration x increases in CdS, the value of the refractive index decreases in the range of 0-5 eV.

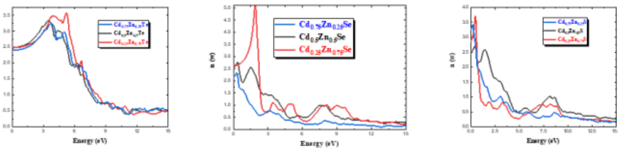

Fig. 9 – Frequency dependent refractive index n of CdZnX (S, Se and Te)

The extinction coefficients $k(\omega)$ of CdZnX (S, Se and Te) has been estimated for each composition x ($0.25 \leq x \leq 0.75$) using Figure 9 data. Consequently, as the concentration of Zn is increased, the peak shifts towards lower energies.

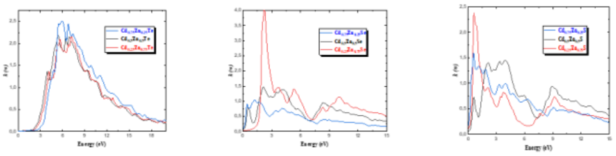

Fig. 10 – Frequency dependent coefficient extinction k of CdZnX (S, Se and Te)

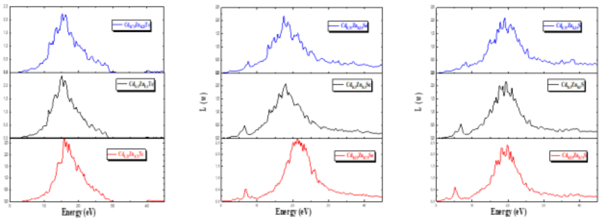

Fig. 11 – Energy loss function of CdZnX (S, Se and Te)

The propagation loss of light inside the material is assessed using the electron energy loss function. The latter, gives relevant information about the elastically scattered and un-scattered electrons along with the number and type of electrons hitting the atom by the light beam. The electron energy loss function of CdZnX (S, Se and Te) is plotted in Figure 11, showing that no scattering occurs at an energy below the band gap. However, outside the transparent region will cause strong polarization, which can lead to chromatic dispersion [19]. The correlation between the refractive index or the absorption coefficient and the propagation loss increase. In the middle energy range, the loss is the largest as inelastic scattering is observed [20]. Additionally, the energy value reaches about 16 eV for CdZnTe, 20 for CdZnSe and 20 for CdZnS . These energy loss spectrum peaks are related to Plasmon resonance, corresponding to the plasma frequency [21]. Materials above this frequency exhibit metallic typical behavior, while materials below this frequency exhibit dielectric properties.

The study also considers the dielectric function $\varepsilon(\omega)$ shown in Figure 12 and Figure 13 for CdZnX (S, Se and Te), which is possibly used for defining the system's linear response to electromagnetic radiation. Thus, the photons-electrons interaction [22]. The $\varepsilon_2(\omega)$ shown in Figure 13 is known as the imaginary part of the dielectric functions. This part is estimated using momentum matrix elements between occupied and unoccupied wave functions Selection Rules for Dielectrics and Real Part $\varepsilon_1(\omega)$ Figure 9. The function follows the Kramer-Kronig correlation. Moreover [23], a significant feature of $\varepsilon_1(\omega)$ is the zero-frequency limit $\varepsilon_1(\omega)(0)$ which indicates the electronic device has partial static permittivity. Therefore, corresponding to each combination x, the optical static dielectric constant (ε_0) of $Cd_{1-x}Zn_xTe$ are 5.80, 6.26 and 6.20 respectively [24]. The real part's main peaks for $Cd_{1-x}Zn_xTe$ are observed at 4.86, 4.31 and 5.11 eV for $x = 0.25$, 0.5 and 0.75 respectively. The optical static dielectric constant (ε_0) of $Cd_{1-x}Zn_xSe$ equals 7.44, 6.62 and 6.93 respectively [70, 85, 86]. The main peaks of the real part of $Cd_{1-x}Zn_xSe$ occur at 0.82, 1.48 and 1.82 eV for $x = 0.25$, 0.5 and 0.75 respectively. The optical static dielectric constant (ε_0) of $Cd_{1-x}Zn_xS$ is found to be 9.59, 6.37 and 7.52 respectively. The main peaks of the real part for $Cd_{1-x}Zn_xS$ occur at 0.79, 1.42 and 0.45 eV for $x = 0.25$, 0.5 and 0.75 respectively.

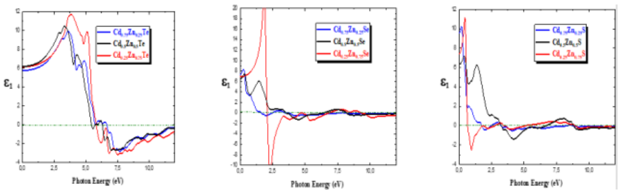

Fig. 12 – Calculated real ε_1 spectra parts of the frequency dependent dielectric functions for CdZnX (S, Se and Te)

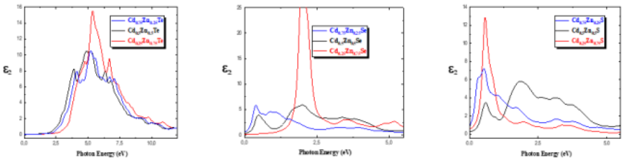

Fig. 13 – Calculated imaginary ε_2 spectra parts of the frequency dependent dielectric functions for CdZnX (S, Se and Te)

5. CONCLUSION

In summary, we report a theoretical investigation of the energy band gap of $Cd_{1-x}Zn_xTe$, $Cd_{1-x}Zn_xSe$, $Cd_{1-x}Zn_xS$ alloys in the whole composition range based on the FP-LAPW method within Tran Blaha-modified Becke-Johnson exchange potential. We find a striking nonlinear dependence in these alloys with bowing parameters ranging from $b = 0.46 - 0.7$ eV for both GGA and LDA calculations. The origin of this bowing was discussed in the highlight of the Zunger approach, which decomposes the bowing effect into three main contributions: structural, electronic and interplay between both. We conclude that volume deformation was the main reason for the bowing effect in this alloy's family.

REFERENCES

1. O. Zelaya-Angel, M. Becerril, J.G. Mendoza-Alvarez, L. Tirado, H. Navarro-Contreras, *J. Appl. Phys.* **95**, 6284 (2004).
2. Manuele Bettelli, et al., *Sci. Rep.* **10** No 1, 13762 (2020).
3. Tooru Tanaka, et al., *J. Crystal Growth* **378**, 259 (2013).
4. Subhash Chander, et al., *Physica E: Low-Dimensional Systems and Nanostructures* **89**, 29 (2017).
5. Zinoviia Tsybrii, et al., *J. Crystal Growth* **529**, 125295 (2020).
6. Khalid Bashir, et al., *Mater. Lett.* **304**, 130737 (2021).
7. Ritika Sharma, et al., *Mater. Res. Bull.* **163**, 112214 (2023).
8. G.G. Rusu, M. Rusu, M. Girtan, *Vacuum* **81**, 1476 (2007).
9. K.H. Kim, Y.H. Na, Y.J. Park, T.R. Jung, S.U. Kim, J.K. Hong, *IEEE Trans. Nucl. Sci.* **51**, 3094 (2004).
10. M. Becerril, O. Zelaya-Angel, R. Fragoso-Soriano, L. Tirado-Mejia, *Rev. Mex. Fis.* **50**, 588 (2004).
11. Y. Jeon, H.S. Kang, *Opt. Rev.* **14**, 373 (2007).
12. S. Stolyarova, F. Edelman, A. Chack, A. Berner, P. Werner, N. Zakharov, M. Vytrykhivsky, R. Beserman, R. Weil, Y. Nemirovsky, *J. Phys. D: Appl. Phys.* **41**, 065402 (2008).
13. Andrea Zappettini, *Single Cryst. Electron. Mater.*, 273 (2019).
14. J. Zázvorka, et al., *J. Lumin.* **143**, 382 (2013).
15. H.P. Hsu, et al., *J. Crystal Growth* **534**, 125491 (2020).
16. Muhammad Ashraf, et al., *Mater. Today: Proc.* **2** No 10, 5695 (2015).
17. Fei Yan, et al., *J. Mater. Res.* **27** No 8, 1112 (2012).
18. C. Tian, R. Tang, S. Hu, W. Li, L. Feng, J. Zhang, L. Wu, *Adv. Mater. Res.* **225–226**, 784 (2011).
19. Jae-Hyeong Lee, Woo-Chang Song, Jun-Sin Yi, Kea-Joon Yang, Wun-Dong Han, Joon Hwang, *Thin Solid Films* **431–432**, 349 (2003).
20. M.S. Hossain, M.A. Islam, Q. Huda, M.M. Aliyu, T. Razykov, M.M. Alam, Z.A. AlOthman, K. Sopian, N. Amin, *Thin Solid Films* **548**, 202 (2013).
21. M.S. Hossain, M.A. Islam, M.M. Aliyu, P. Chelvanathan, T. Razykov, K. Sopian, N. Amin, *Energy Procedia* **33**, 214 (2013).
22. S.D. Chavhan, S. Senthilarasu, Soo-Hyoung Lee, *Appl. Surf. Sci.* **254**, 4539 (2008).
23. J-H. Lee, W-C. Song, J-S. Yi, K-J. Yang, W-D. Han, J. Hwang, *Thin Solid Films* **431–432**, 349 (2003).
24. K.R. Murali, M. Balasubramanian, *Curr. Appl. Phys.* **10**, 734 (2010).

Дослідження параметрів викривлення забороненої зони, електронних та оптичних властивостей напівпровідникових сплавів $Cd_{1-x}Zn_xTe$, $Cd_{1-x}Zn_xS$ та $Cd_{1-x}Zn_xS$ методом розрахунку з перших принципів

K. Mimouni[1], K. Beladjal[1], Slimane Latreche[2], Charef Azzeddine[1,3], A. Benzetta[4], M. Abderrezek[5], N. Mokdad[1], Benramache Said[3]

[1] *Laboratoire d'Étude des Matériaux Optoélectronique & Polymères, Physics Department, University Oran1, Ahmed Ben Bella, BP1524 El M'naour, Oran, Algeria*

[2] *Technical Platform for Physico-Chemical Analysis (PTAPC), Microstructural and Microanalysis Division, University of Science and Technology (USTHB), BP 32 El-Alia, Bab-Ezzouar, Algiers 16111, Algeria*

[3] *Laboratoire de Physique Photonique et Nanomatériaux Multifonctionnels, LPPNM, Biskra University, Biskra 07000 Algeria*

[4] *Higher School of Signals (HSS), Po Box 11, Kolea, 42070, Tipaza, Algeria*

[5] *Unité de Développement des Equipements Solaires, UDES / Centre de Développement des Energies Renouvelables, CDER, 42415Tipaza, Algérie*

У цьому дослідженні було проведено детальне вивчення ширини заборонених зон у напівпровідникових сплавах, зокрема $Cd_{1-x}Zn_xTe$, $Cd_{1-x}Zn_xSe$ та $Cd_{1-x}Zn_xS$, всі з яких мають кристалічну структуру цинкової суміші. Для проведення нашого аналізу ми використовували метод лінеаризованої доповненої плоскої хвилі з повним потенціалом (FP-LAPW), застосовуючи як узагальнене градієнтне наближення (GGA), так і наближення локальної густини (LDA) для досягнення точних результатів. Для точного визначення ширини заборонених зон та параметрів вигинання спиралися на модифікований обмінний потенціал Бекке-Джонсона Тран-Блаха (TB-mBJ), відомий своєю ефективністю в розрахунках зонних структур. Результати показали помірно нелінійну залежність значень ширини забороненої зони від складу, з параметрами вигинання, оціненими приблизно як $b \approx 0{,}49$ еВ для $Cd_{1-x}Zn_xTe$, $b \approx 0{,}68$ еВ для $Cd_{1-x}Zn_xS$ та $b \approx 0{,}63$ еВ для $Cd_{1-x}Zn_xSe$. Ця спостережувана нелінійність була головним чином пов'язана з ефектами об'ємної деформації, згідно з підходом Цунгера, який пояснює, як структурні спотворення можуть впливати на електронні властивості. Окрім аналізу ширини забороненої зони, досліджені ключові оптичні властивості, включаючи коефіцієнт поглинання, показник заломлення, відбивну здатність, функцію втрат енергії та силу осцилятора. Ці оптичні характеристики пропонують глибше розуміння електронних структур матеріалів та їхньої реакції на світло. Спостерігали збільшення ефективного числа електронів під час фотозбудження зі зростанням концентрації Zn, що вказує на підвищену оптичну активність у цих сплавах. Це дослідження проливає світло як на електронні, так і на оптичні властивості, що робить ці сплави $Cd_{1-x}Zn_xTe$, $Cd_{1-x}Zn_xS$ та $Cd_{1-x}Zn_xS$ перспективними кандидатами для оптоелектронних застосувань, де точне налаштування ширини забороненої зони та оптичних відгуків є важливим для оптимальної роботи пристрою.

Ключові слова: Енергетична заборонена зона, Параметри вигинів, Оптичні властивості, Напівпровідники II-VI групи, Модифікований обмінний потенціал Бекке-Джонсона за Тран-Блахою.